nature materials

LETTERS

https://doi.org/10.1038/s41563-018-0062-0

Motorizing fibres with geometric zero-energy modes

Arthur Baumann[1], Antoni Sánchez-Ferrer[2], Leandro Jacomine[1], Philippe Martinoty[1], Vincent Le Houerou[1], Falko Ziebert[1,3]* and Igor M. Kulić[1]*

Responsive materials[1–3] have been used to generate structures with built-in complex geometries[4–6], linear actuators[7–9] and microswimmers[10–12]. These results suggest that complex, fully functional machines composed solely from shape-changing materials might be possible[13]. Nonetheless, to accomplish rotary motion in these materials still relies on the classical wheel and axle motifs. Here we explore geometric zero-energy modes to elicit rotary motion in elastic materials in the absence of a rigid wheel travelling around an axle. We show that prestrained polymer fibres closed into rings exhibit self-actuation and continuous motion when placed between two heat baths due to elastic deformations that arise from rotational-symmetry breaking around the rod's axis. Our findings illustrate a simple but robust model to create active motion in mechanically prestrained objects.

Smart materials that respond to light[11,14–18], thermal[12], electric[3,7] or osmotic stresses[9,19,20] can be operated as simple linear actuators. However, the concepts of classical mechanical machines seem far richer and extend beyond the reversible motions generated by these artificial materials. To build truly complex continuum machines it is inevitable to think beyond the material properties and reflect on sample geometry, topology and symmetry.

A notable principle from condensed matter physics states that whenever a continuous symmetry of a system is broken, a zero wavenumber, zero frequency 'hydrodynamic' mode emerges[21,22]. Classical examples are the nematic phase in liquid crystals and the ordered spin phase in the XY model[21] in which the rotational symmetry is broken by the preferred director or spin orientation. With no energy cost to rotate the molecules or spins collectively, the corresponding long wavelength distortion becomes a new hydrodynamic variable in the system. Generalizing the concept to elastic solids, here we propose a model, termed the 'embedded wheel', that allows the generation of soft motors into responsive materials. The idea is to induce and actively drive continuum-elastic modes in objects that bear internally trapped mechanical prestrains.

Consider the simplest of such objects, an elastic rod closed into a circular loop (Fig. 1a). By the process of closure, the initially cylindrical rod, now bent into a torus, displays topological prestrain and a broken symmetry—the inner side experiences longitudinal compression, whereas the outer part is subject to tension (Fig. 1a). As in the hydrodynamic-mode scenario, the breaking of rotational symmetry around the rod's axis gives rise to a zero-energy mode; this corresponds to turning every cross-section around the long axis of the toroid (Fig. 1b). This collective deformation represents an embedded wheel that in an ideal elastic material, without defects and viscous losses, becomes a true zero-energy mode.

Such global zero-elastic-energy modes (ZEEMs) are not restricted to the toroidal geometry[22,23] and are surprisingly common (Fig. 1c): from wrinkles on surfaces[24], ripples on edge-stressed sheets[7,24], isometric excess-angle cones[25] and Möbius strips[26] to plectonemic supercoils 'slithering' along closed DNA molecules[27].

Although ZEEMs resemble rigid rotations in that they conserve both the energy and the outer form of the object, they form a distinct class of motion that involves continuum material deformations. A particularly useful feature is their potential to be actively driven by dissipative self-organization. As a proof of concept, we demonstrate this effect in a simple ZEEM model system—a toroidal polymer fibre between two heat baths that undergoes (non-rigid) rotation, performs mechanical work, stores energy and self-propels.

To drive the toroidal fibre actively, we utilize the idea of generating a mechanically frustrated dynamic steady state within the fibre's cross-section. For this, we placed a thin elastic rod of circular cross-section closed into a circular loop on a heating plate (Fig. 2b). The temperature gradient between the plate and the ambient air (along the z direction) induces a thermal strain difference in the fibre's cross-section, normal to the geometrically induced strain (which is in-plane, along x; see Fig.2a). Clearly, it would be energetically preferential for the system to align its thermally compressed/expanded regions to those already compressed/expanded in the inner/outer circumference of the torus. However, as the thermal strain is externally driven—and maintained—a dynamic frustration emerges and a torque around the fibre's axis is generated. If this driving torque overcomes the prevalent dissipation processes, a continuous internal rotation sets in, the ZEEM becomes mobile and the embedded wheel turns (Fig. 2c). Figure 2d,e demonstrates the mechanism in probably the simplest-imaginable motors with only one moving component—and no stator—made by closing a fibre from either polydimethylsiloxane (PDMS) rubber or nylon into a ring. As nylon is thermally contracting upon heating, rotation is in the inwards direction (Fig. 2c,e), whereas PDMS rings rotate in the opposite direction (Fig. 2d) due to their positive thermal expansion coefficient.

To understand the phenomenon, we developed a simple model that accounts for the fibre's elasticity, dissipation and externally driven temperature profile. For a fibre with Young's modulus Y, cross-sectional radius R and an externally prescribed curvature κ, the induced driving torque per unit length $m \approx YR^3\kappa z$ can be understood as the product of the geometrically imposed strain $\sim R\kappa$ and the thermally induced stress $\sim Yz$ integrated over the cross-section $\sim R^2$. The dynamic variable $z = \alpha_{||}\Delta T_z$ is the thermal strain difference in the direction normal to the plane with $\alpha_{||}$ the thermal expansion coefficient along the fibre axis and ΔT_z the temperature difference from top to bottom (Fig. 2b). From an advection–diffusion equation

[1]Institut Charles Sadron UPR22-CNRS, Strasbourg Cedex 2, France. [2]Department of Health Sciences & Technology (D-HEST), Swiss Federal Institute of Technology (ETH Zürich), Zürich, Switzerland. [3]Institute for Theoretical Physics, Ruprecht-Karls-University, Heidelberg, Germany. *e-mail: f.ziebert@thphys.uni-heidelberg.de; kulic@unistra.fr

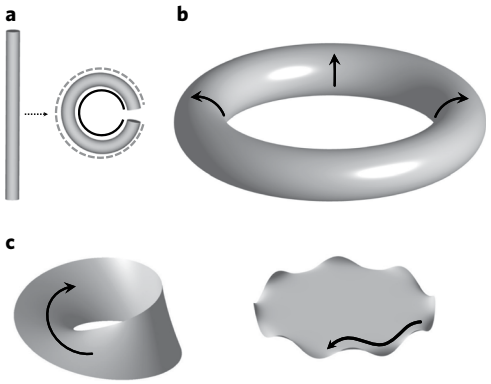

Fig. 1 | Global ZEEMs in prestrained elastic objects. a, Closing an elastic rod into a circular loop induces a compressive strain in the inner portion (solid line) and tensile strain on the outside (dashed line). **b**, The elastic torus now has a deformation mode that leaves its energy and external form invariant. **c**, Various other elastic objects, such as the Möbius strip and an edge-crumpled disk, possess global ZEEMs.

for the temperature distribution (Supplementary Methods gives details) one obtains equations for the thermal strain differences parallel ($x = \alpha_{\parallel}\Delta T_x$) and normal ($z$) to the plane,

$$\dot{x} = -x/\tau - \omega z,\ \dot{z} = p - z/\tau + \omega x \qquad (1)$$

Here τ is a characteristic thermal relaxation time of the cross-section. The thermal strain difference in the normal direction, z, is actively driven by the external temperature difference $\Delta T_{ext} = T_s - T_{air}$ (between the surface of the hot plate and the surrounding colder air) via a strain-pumping rate $p \propto \alpha_{\parallel}\Delta T_{ext}$. Both τ and p are functions of the system parameters (for example, fibre radius and thermal diffusivity). The embedded wheel corresponds to the continuous turnover between x and z via the angular frequency ω. Once the continuous rotation sets in, the balance of torques reads $m = m_{dissip}$ with m_{dissip} the dissipative torque, which consists of dry friction and the viscous dissipation in the material (Supplementary Methods).

The fibre closed into a torus constitutes a unidirectional motor: the turning direction is dictated by the geometry of closure and the sign of the thermal expansion coefficient (Fig. 2d,e) The onset of motion is continuous in the driving temperature, that is, motion starts from zero angular frequency at a threshold (Fig. 2f). The toroidal fibre motors are very robust and failure resistant and turn for tens of hours up to days (Supplementary Methods). In fact, they even display a form of dynamic self-healing: the cooperative rotation of the full fibre length allows local defects along the contour to be progressively smoothed out during the motor's operation (Supplementary Video 6).

The toroidal motors are elegant self-contained devices, but difficult to interconnect due to their closed geometry. We found that fibre rotation persists even when the curvature is externally imposed. With the use of a holding set-up, fibres were forced into a spiral path, as shown in Fig. 3a, an arrangement that can be seen as a parallel connection of many concentric partial toroidal motors. Figure 3b demonstrates the device's ability to lift macroscopic loads—a 3 m nylon fibre of 1.5 g lifted 20 g. Spirals are able to exert large torques because all the cross-sections work cooperatively. Moreover, when rigidly stalled and prevented from rotating at one end, the 'spiral fibre motor' is able to store torsional energy by a rotation of the

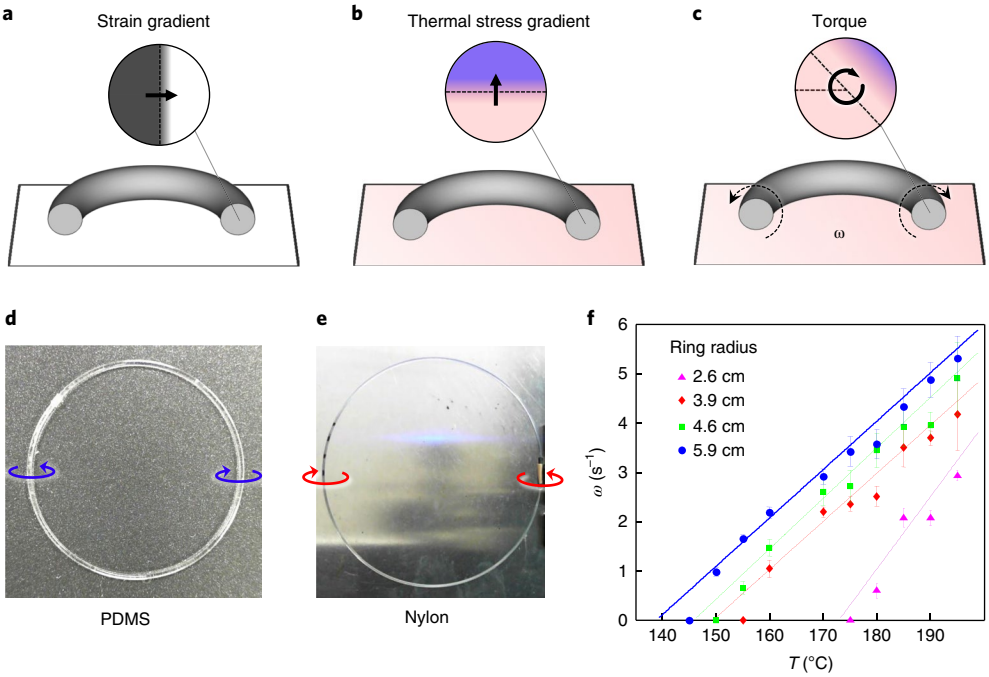

Fig. 2 | Self-organized driving of ZEEMs. a, The strain induced by bending has a gradient in the torus plane. **b**, When placed between a hot surface and the ambient air, a temperature gradient develops along the z direction (perpendicular to the plane) and gives rise to thermal prestrains in the same direction. **c**, The incompatibility of the geometrically imposed and thermally driven strains (**a** and **b**) leads to a dynamic instability—the torus begins to turn with constant angular frequency ω. The direction of rotation depends on the sign of the thermal expansion coefficient (the sketched case shows a negative thermal expansion, as for nylon). **d**, A PDMS fibre closed in a ring (radius 2 cm, fibre thickness 0.6 mm) on a hot plate (175 °C) becomes a robust unidirectional motor. **e**, A nylon fibre closed into a ring (radius 6 cm) by a small brass tube rotates in the opposite direction. **f**, The angular frequency of various-sized nylon rings (fibre thickness 0.6 mm) as a function of plate temperature. Error bars: s.d. from ten measurements on the same ring (Supplementary Video 1).

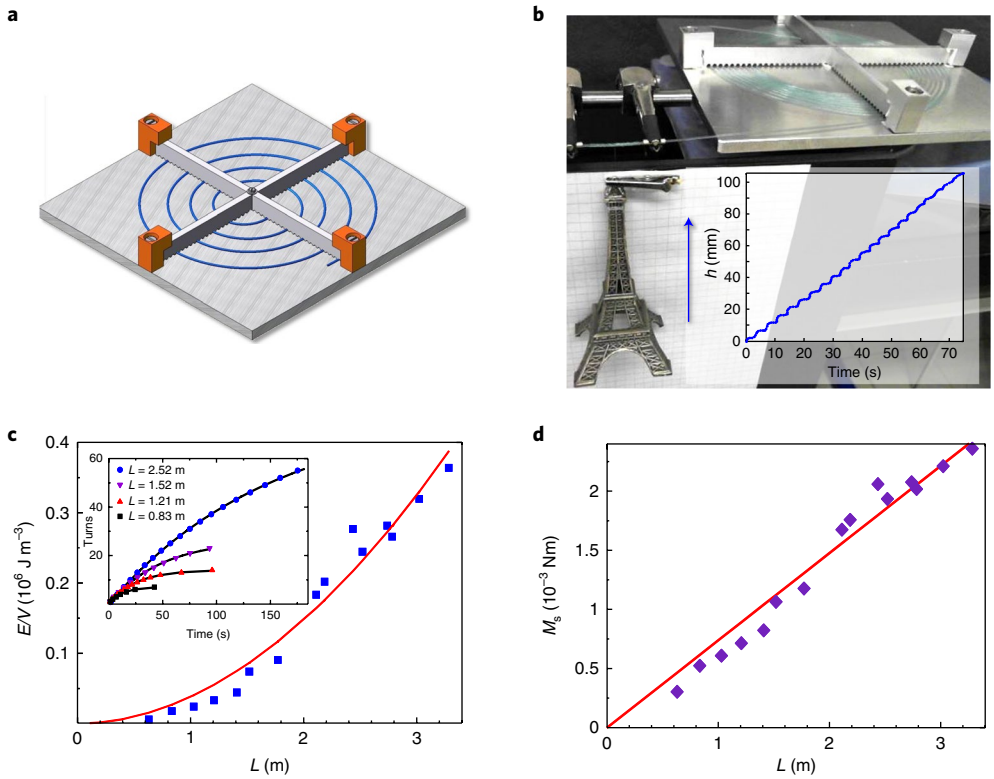

Fig. 3 | The spiral fibre motor. a, A nylon fibre is constrained to a spiral path by an aluminium holder. Upon heating the plate, the whole fibre rotates around its tangent, performing work and/or storing torsional energy. **b**, A spiral motor (fibre thickness 0.8 mm, total spiral length 3.2 m) rotating at 185 °C lifting a payload (Eiffel Tower replica of weight 20 g). The fibre is guided from the spiral holder through two brass tubes and rotates freely there. Inset: position of the weight as it is lifted (Supplementary Video 2). **c**, Charging of the 'spiral fibre battery'. Inset: number of turns as a function of time for spirals of various lengths that are rigidly blocked at one end. The lines are fits to the theory (Supplementary Methods and Supplementary equation (64)), which allows an estimate of the stored elastic-energy density, shown in the main panel as a function of spiral length. The red line is the predicted scaling with L^2. **d**, The stalling torque of the spirals studied in **c** as a function of spiral length, which displays a linear scaling (red line).

fibre's free end that continues for several minutes and hundreds of turns before stalling (Fig. 3c). This stored torsional elastic energy can later be utilized when the fixed end is released again. With the thermal and elastic torques balanced, for a strong thermal pumping (Supplementary Methods) the stalling torque scales as:

$$M_s \simeq YR^3\kappa\alpha_{\parallel}\Delta T_{ext}L \quad (2)$$

and the stored torsional energy density of a blocked motor as:

$$\frac{E}{V} \simeq Y\kappa^2(\alpha_{\parallel}\Delta T_{ext})^2L^2 \quad (3)$$

where κ the average curvature of the spiral and L its length. Figure 3c shows the estimated energy density obtained by fitting the dynamic solution of a torque balance model to the experimentally measured number of turns (inset). The linear increase of the torque and the quadratic increase of the energy density with the length of the fibre are signatures of the collective interplay of the spiral's gyres. The rapidly growing energy-storage capacity is only limited by the mechanical failure point of the fibre or the holding device. The set-up may hence be used as a residual thermal-energy harvesting and storage device. The spiral motor's efficiency can be estimated as $\eta \simeq \frac{M_s\omega}{\dot{Q}} \simeq 10^{-3}$, where $\dot{Q} \simeq 2RLh\Delta T_{ext}$ is the heat current through the fibre per unit time, with h the heat transfer coefficient at the fibre–air interface, and $M_s\omega$ is the useful power output.

For the toroidal and spiral fibres, the ZEEM is imposed by topology and external constraints, respectively. Interestingly, even initially straight fibres can develop a self-organized zero mode. When straight fibres were placed on a hot substrate, we observed a rapid self-propulsion via a rolling motion orthogonal to the fibre's long axis at typical speeds of centimetres per second (Fig. 4a,b).

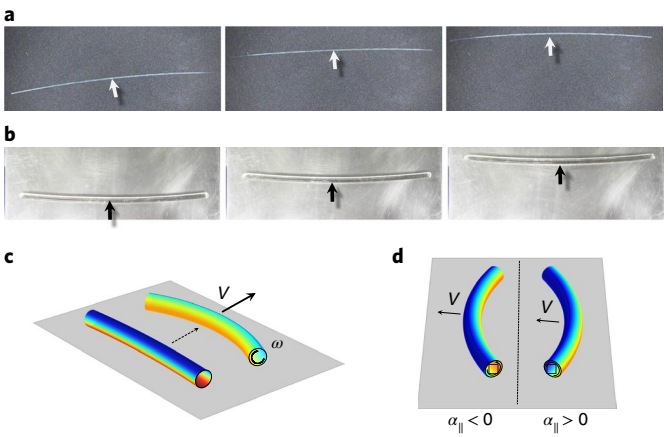

Fig. 4 | Spontaneous symmetry breaking and self-propulsion of linear fibres. a,**b**, Rolling motion of a nylon-6 rod (diameter 0.6 mm, length 12 cm) (**a**) and a PDMS rod (diameter 3 mm, length 11 cm) (**b**). **c**, The thermal gradient induces a curving via thermal expansion and/or contraction. The temperature is hot (red) or cold (blue). Due to the confinement (on the plate) the curving stays in-plane, which effectively creates a torque. **d**, The direction of the torque and the rolling velocity V depends on the sign of the material's thermal expansion coefficient (Supplementary Videos 3 and 5).

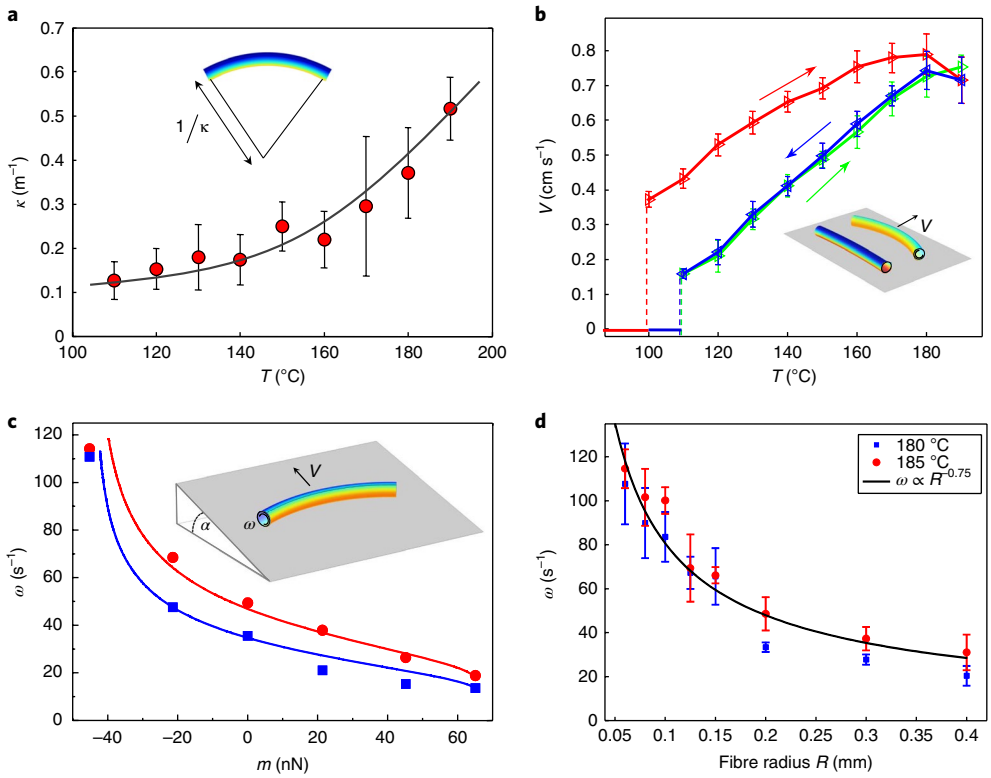

Fig. 5 | Fibre rotation and rolling motion. a, Thermally induced curvature as a function of temperature for a nylon-6 fibre of radius 0.3 mm. **b**, Rolling velocity (same fibre as in **a**). During the first temperature cycle (red line), the fibre undergoes an annealing process and becomes conditioned ('trained'). In the subsequent cycles of decreasing/increasing temperature, the fibre attains a reproducible velocity (blue/green curves). **c**, Single fibres are bidirectional motor units able to perform work, in the experiment shown here it is against their own weight on an inclined plane. Shown is the angular turning frequency of a nylon-6 fibre (0.2 mm radius) as a function of the axial torque at two different temperatures (red, 180 °C; blue, 140 °C). Solid lines are fits to the theoretically predicted torque–velocity relation (Supplementary Methods). **d**, Fibres with decreasing radii rotate with increasing angular frequencies: experimental data for two temperatures and a power-law fit $R^{-\gamma}$ with $\gamma = 0.75$. Error bars (**a**, **b** and **d**): s.d. from three independent fibre specimens.

This motion is governed by the same principle (and the same equations) with the difference that now the curvature is not externally imposed but thermally induced; it is given by $\kappa = -x/R$, where $x = \alpha_{\|}\Delta T_x$ is the in-plane thermal strain difference that results from the in-plane temperature difference ΔT_x that emerges spontaneously via rotational advection (Fig. 4c and Supplementary Methods). In fact, the fibres are slightly, but visibly, curved when self-propelling (Fig. 5a). At the onset, one of the two possible in-plane curving directions is spontaneously chosen. The model explains the relation between the rolling direction and the curvature direction: fibres that exhibit a negative axial thermal expansion (like nylon-6) move in the opposite direction from their centre of curvature, whereas those with a positive thermal expansion (like PDMS) move towards their centre of curvature (Fig. 4d).

Typical turning frequencies are higher (0.5–20 Hz) than for the torus, as internal dissipation is negligible due to the small curvature, and a small rolling-type friction dominates. As for the torus, below a threshold temperature no motion is observed, but now the onset is discontinuous (first order), that is, setting-in with a finite velocity (Fig. 5b). This difference can be understood to originate from the symmetry being already broken for the torus while being self-organized for the fibre (Supplementary Methods). The direction of rolling, initially chosen spontaneously, can change in the course of time, for instance, due to collisions with surface defects or larger objects on the plate. Hence, rolling fibres are bidirectional motors, but nylon fibres especially roll very persistently for high temperatures. The torques exerted are sufficiently large to allow fibres to roll uphill on an inclined plane (of slopes of up to 15°) (Fig. 5c) The torque–angular frequency relation obtained using the model shows a good agreement with experiment. Finally, another important property of the rolling fibre can be unravelled from a study of speed versus fibre thickness (Fig. 5d): the rotation frequency strongly increases with decreasing fibre radius, reaching 20 Hz for the thinnest fibres tested (60 µm radius). These high frequencies stand out among thermally driven smart materials and are comparable to the beating frequency of cilia[28] and the fastest light-driven azobenzene oscillators[17,18]. The deformation flux through the fibres shares some similarity with evaporating Leidenfrost droplets[29,30] but, in contrast to them, it does not consume the sample as it emerges and propagates within a solid material.

We have proposed a concept termed 'wheel within the material' and demonstrated its practical feasibility using mundane polymer fibres. Toroidal, spiral and even linear fibres turn into robust, one-piece motors when driven away from equilibrium due to dynamic frustration that emerges within the material. ZEEMs in materials are ubiquitous and generating dynamic frustration to drive them can be as easy as placing spaghetti on a hot stove (Supplementary Video 3). The underlying model suggests that many other driving mechanisms should potentially induce rotation; in fact, the energy pumping rate (p), here related to a heat flux, could be substituted by any flux normal to the plane and coupling to the strain. The insight that we can now dispense with the ancient wheel and axle and utilize intrinsic ZEEMs instead opens exciting new perspectives on soft machines. The ZEEM motors, made from mundane plastic, rubber and starch, call for rethinking the very meaning of a smart material and shift the spotlight from microscopic material properties to sym-

metry and topology. Through them, the material acquires a form of collective smartness that resides in none of its individual parts, yet is globally encoded in their delicate interplay.

Methods

Methods, including statements of data availability and any associated accession codes and references, are available at https://doi.org/10.1038/s41563-018-0062-0.

Received: 12 May 2017; Accepted: 20 March 2018;
Published online: 30 April 2018

References

1. de Gennes, P. G. Reflexions sur un type de polymères nematiques. *C.R. Acad. Sci. Paris B* **281**, 101–103 (1975).
2. Küpfer, J. & Finkelmann, H. Nematic liquid single crystal elastomers. *Macromol. Chem. Rapid Commun.* **12**, 717–726 (1991).
3. Tanaka, T., Nishio, I., Sun, S.-T. & Ueno-Nishio, S. Collapse of gels in electric field. *Science* **218**, 467–469 (1982).
4. Klein, Y., Efrati, E. & Sharon, E. Shaping of elastic sheets by prescription of non-Euclidean metrics. *Science* **315**, 1116–1120 (2007).
5. Kim, J., Hanna, J. A., Byun, M., Santangelo, C. D. & Hayward, R. C. Designing responsive buckled surfaces by halftone gel lithography. *Science* **335**, 1201–1205 (2012).
6. Pezzulla, M., Shillig, S. A., Nardinocchi, P. & Holmes, D. P. Morphing of geometric composites via residual swelling. *Soft Matter* **11**, 5812–5820 (2015).
7. Pelrine, R., Kornbluh, R., Pei, Q. & Joseph, J. High-speed electrically actuated elastomers with strain greater than 100%. *Science* **287**, 836–839 (2000).
8. Haines, C. S. et al. Artificial muscles from fishing line and sewing thread. *Science* **343**, 868–872 (2014).
9. Mirfakhrai, T., Madden, J. D. W. & Baughman, R. H. Polymer artificial muscles. *Mater. Today* **10**, 30–38 (2007).
10. Dreyfus, R. et al. Microscopic artificial swimmers. *Nature* **437**, 862–865 (2005).
11. Camacho-Lopez, M., Finkelmann, H., Palffy-Muhoray, P. & Shelley, M. Fast liquid–crystal elastomer swims into the dark. *Nat. Mater.* **3**, 307–310 (2004).
12. Mourran, A., Zhang, H., Vinokur, R. & Möller, M. Soft microrobots employing nonequilibrium actuation via plasmonic heating. *Adv. Mater.* **29**, 1604825 (2016).
13. Palagi et al. Structured light enables biomimetic swimming and versatile locomotion of photoresponsive soft microrobots. *Nat. Mater.* **15**, 647–653 (2016).
14. Yamada, M. et al. Photomobile polymer materials: towards light-driven plastic motors. *Angew. Chem. Int. Ed.* **47**, 4986–4988 (2008).
15. Ikegami, T., Kageyama, Y., Obara, K. & Takeda, S. Dissipative and autonomous square-wave self-oscillation of a macroscopic hybrid self-assembly under continuous light irradiation. *Angew. Chem. Int. Ed.* **55**, 8239–8243(2016).
16. White, T. J. et al. A high frequency photodriven polymer oscillator. *Soft Matter* **4**, 1796-8 (2008).
17. Zhang, X. et al. Photoactuators and motors based on carbon nanotubes with selective chirality distributions. *Nat. Commun.* **5**, 2983 (2014).
18. Ionov, L. Hydrogel-based actuators: possibilities and limitations. *Mater. Today* **17**, 494–503 (2014).
19. Ma, M., Guo, L., Anderson, D. G. & Langer, R. Bio-inspired polymer composite actuator and generator driven by water gradients. *Science* **339**, 186–189 (2013).
20. Martin, P. C., Parodi, O. & Pershan, P. S. Unified hydrodynamic theory for crystals, liquid crystals, and normal fluids. *Phys. Rev. A* **6**, 2401–2420 (1972).
21. Chaikin, P. & Lubensky, T. *Principles of Condensed Matter Physics* (Cambridge Univ. Press, Cambridge, 1995).
22. Kulić, I. M., Thaokar, R. & Schiessel, H. Twirling DNA rings, swimming nanomotors ready for a kickstart. *Europhys. Lett.* **72**, 527–533 (2005).
23. Bhattacharya, K. & James, R. D. The material is the machine. *Science* **307**, 53–54 (2005).
24. Audoly, B, . & Pomeau, Y. *Elasticity and Geometry* (Oxford Univ. Press, Oxford, 2010).
25. Müller, M. M., Ben Amar, M. & Guven, J. Conical defects in growing sheets. *Phys. Rev. Lett.* **101**, 156104 (2008).
26. Starostin, E. L. & van der Heijden, G. H. M. The shape of a Möbius strip. *Nat. Mater.* **6**, 563–567 (2007).
27. Marko, J. F. The internal 'slithering' dynamics of supercoiled DNA. *Phys. A* **244**, 263–277 (1997).
28. Satir, P. Studies on *Cilia*. *J. Cell Biol.* **39**, 77–94 (1968).
29. Bormashenko, E. et al. Self-propulsion of liquid marbles: Leidenfrost-like levitation driven by Marangoni flow. *J. Phys. Chem. C* **119**, 9910–9915 (2015).
30. Linke, H. et al. Self-propelled Leidenfrost droplets. *Phys. Rev. Lett.* **96**, 154502 (2006).

Acknowledgements

The authors acknowledge the Micro Nano Mechanics at ICS for providing the DMTA facility and thank A. Dutta for useful comments. This work was supported in part by the ANR grant Integrations.

Author contributions

A.B., A.S.-F., L.J., V.L.H., P.M. and I.M.K. performed the experiments and analysed data, I.M.K. conceived the work, F.Z. and I.M.K. developed the theory, designed the experiments and wrote the paper, and all the authors commented on the article.

Competing interests

The authors declare that they have no competing interests.

Additional information

Supplementary information is available for this paper at https://doi.org/10.1038/s41563-018-0062-0.

Reprints and permissions information is available at www.nature.com/reprints.

Correspondence and requests for materials should be addressed to F.Z. or I.M.K.

Publisher's note: Springer Nature remains neutral with regard to jurisdictional claims in published maps and institutional affiliations.

Methods

Sample preparation and characterization. We tested several types of polymeric materials and observed that both structurally anisotropic and semicrystalline (nylon-6 and polyvinylidene difluoride (PVDF)) as well as isotropic and amorphous polymeric samples (starch, silicone rubber and PDMS) display the motile ZEEM effect. Interestingly, a classical thermo-actuating metallic material, like a nickel–titanium (nitinol) fibre, did not show rotary motion, which pinpoints the importance of a low thermal conductivity to maintain the necessary temperature gradients.

The most robust samples were found to be nylon-6 fishing-line fibres. They were gently annealed (Fig. 5b, Supplementary Methods and Supplementary Video 4) to remove built-in prestress that stemmed from their fabrication process before displaying a very reproducible velocity–temperature dependence. Wide-angle X-ray scattering characterization of the samples (Supplementary Methods) shows a polymorphic order-to-order (alpha–-gamma) transition within the crystalline domains as the origin of the large anisotropic thermal contraction with a negative expansion coefficient along the fibre axis of $\alpha_{\parallel} = -1.9 \times 10^{-4}\,K^{-1}$ between 120 and 180 °C.

The samples made of PDMS were prepared form a two-part kit that consisted of liquid components (Rhodorsil RTV141 A+B (Bluestar)). The base and curing agents were mixed in a weight ratio of ten parts base to one part curing agent with stirring for about 2 min. The cross-linked samples were obtained by moulding the mixture after removing air bubbles by vacuum processing for 30 min. The final PDMS filaments were formed in glass tubes (capillaries and glass pipettes) that were gently fragmented after the curing process, which lasted for 2 h at 80 °C. The so-prepared PDMS rubber has a longitudinal expansion coefficient of $\alpha_{\parallel} = +3.3 \times 10^{-4}\,K^{-1}$.

The PDMS, PVDF and nylon rings were held together with short pieces of thermocontracting PVDF shrink tubes or metallic brass tubes.

Data availability. The data sets generated during and/or analysed during the current study are available from the corresponding author on reasonable request.